Gómez-Hernández, J., González-Gómez, P. A., Briongos, J. V. & Santana, D. (2018). Influence of the steam generator on the exergetic and exergoeconomic analysis of solar tower plants. *Energy*, 145, pp. 313–328.

DOI: 10.1016/j.energy.2017.12.129

Influence of the steam generator on the exergetic and exergoeconomic analysis of solar tower plants

J. Gómez-Hernández*[1], P. A. González-Gómez[1], J. V. Briongos[1], D. Santana[1]

[1]Carlos III University of Madrid (Spain)

Department of Thermal and Fluids Engineering

Avda. de la Universidad 30, 28911, Leganés (Madrid, Spain)

* corresponding author: jegomez@ing.uc3m.es Tel: +34916246034. Fax: +34916249430.

Abstract

Solar power tower plants differ from conventional power plants in the steam generator design due to the higher heat duty. In this work, the influence of the steam generator heat exchangers (preheater, evaporator, superheater and reheater) on a solar power plant with molten salt receiver and thermal storage is studied for the first time. Energy, exergy and exergoeconomic analyses give a complete view of the cost flows within the system. The pinch point temperature difference in the evaporator is used as the main variable as it changes the steam generator design and the operating conditions of the plant, such as the inlet temperature of the receiver and the salt mass flow. All heat exchangers are designed and optimized at minimum cost for each pinch point to fulfill the thermomechanical limitations of TEMA standards and Pressure Vessel code. The field of heliostats, molten-salt receiver and the power-block (110 MWe) designs are kept constant throughout the paper. A low pinch point should be used to minimize the plant exergy destruction while the exergoeconomic approach obtains an optimum pinch point around 2-3ºC. Furthermore, the low exergoeconomic factor values show that the heat exchangers of the SG are crucial for the plant operation.

Keywords: exergy analysis, exergoeconomic analysis, solar power tower plant, steam generator, pinch point, optimization

Nomenclature

Abbreviations

COND	condenser
CT	cold tank
DEA	deaerator
EV	evaporator
FW	feedwater heater
GA	genetic algorithm
HPT	high pressure turbine
HRSG	heat recovery system generator
HT	hot tank
LPT	low pressure turbine
PH	preheater
PP_{EV}	pinch point temperature difference in the evaporator
PUC	purchasing unit cost.
R	receiver
RH	reheater
sCO_2	supercritical CO_2 cycle
SG	steam generator
SF	solar field

SH superheater

SPTP solar power tower plant

TAC total annualized cost

TES thermal energy storage

Symbols:

$A_{aperture}$ aperture area of the solar field (m^2)

C cost ($)

$\dot{C}$ cost rate ($/h)

c unit cost of exergy ($/GJ)

Cp specific heat capacity (J/kgK)

cp construction period (years)

$\dot{E}$ exergy rate (MW)

f exergoeconomic factor (%)

f_{ann} annuity factor (-)

frc capital return factor

F_{view} radiative view factor (-)

g gravity constant (m/s^2)

h enthalpy (J/kg)

H_{opd} operation time (h)

h_R height of the tower (m)

in interest rate (%)

68	*lf*	lifetime of the plant (years)
69	$\dot{m}$	mass flow rate (kg/s)
70	N_{hot}	number of hot start-ups (-)
71	N_{warm}	number of warm start-ups (-)
72	$\dot{Q}$	heat rate (MW)
73	*q*	economic factor (-)
74	*P*	pressure (bar)
75	*ri*	rate of inflation (%)
76	*s*	entropy (J/kgK)
77	*T*	temperature (ºC)
78	*V*	velocity (m/s)
79	$\dot{Z}$	investment, operation and maintenance cost rate ($/h)
80	*z*	height (m)
81	*Greek symbols:*	
82	ε	exergy efficiency
83	ε_e	receiver thermal emittance
84	ΔP	pressure drop (bar)
85	η	efficiency
86	ρ	density (kg/m^3)
87	σ	Stefan-Boltzmann constant
88	φ	maintenance factor

Subscripts

0	dead state
abs	absorbed
ch	chemical
CI	capital investment
conv	convection
D	destructed
i	inlet
e	exit
F	fuel
OM	operating and maintenance
opt	optical
P	product
ph	physical
Q	heat
R	receiver surface temperature
rad	radiation
S	Sun
TTD	terminal temperature difference
W	work

1. Introduction

Renewable energy production employing solar power tower plants (SPTP) has gained much attention to produce electricity at a large scale. These systems are composed by a field of heliostats that concentrates the solar energy to a high-temperature receiver placed on the top of a central tower. Conventional receivers employ molten salt (60% $NaNO_3$ and 40% KNO_3) to absorb the reflected energy on the tower, which is later used in the steam generator to evaporate the water used by a subcritical regenerative Rankine-cycle in the power block. Similarly to other power cycles, the main goal of the SPTP is the energy production maximization at the minimum operation cost. To that end, power thermal cycles have been thermodynamically analyzed to compute the energy efficiency of the overall system. Many efforts have been conducted to understand the processes that lead to the loss of energy [1, 2, 3]. Furthermore, it is possible to combine the energy and exergy results with an economic analysis employing an exergoeconomic approach. In this analysis, the main objective is the calculation of the total cost rate of the system to understand the cost formation process and the flow of costs in the system [4, 5]. The total cost rate is proportional to the costs associated with exergy destruction as well as to the capital investment and the operating and maintenance costs. Thus, it is possible to optimize a power plant by minimizing the total cost rate of the system.

Many works have evaluated the power cycles performance using energy, exergy, exergoeconomic and economic analyses [6]. Focusing on the exergoeconomic approach, several authors have optimized the performance of a power plant by minimizing the capital and the exergy destruction costs. This approach has been carried out for different fuels [7], several cogeneration schemes [8] and a steam power plant [9]. In particular, the results of [9] showed the relevance of the boiler, which destroys the maximum exergy rate at the maximum cost flow. Similarly, two different approaches were proposed by Carapellucci et al. [10] for the optimization of several layouts of combined cycle gas turbines. The first minimizes the cost per unit of

electricity generated, while the second is focused on reducing the total cost rate of exergy destruction. The different layouts explored the optimum configuration of the plant as a function of the pinch point (PP_{EV}). The results show that the operating parameters of the heat recovery system generator (HRSG) depend on the optimization methodology when analyzing the overall system, although similar results are obtained using both methods if the analysis is limited to the HRSG. The relevance of the HRSG is also studied in a similar work changing the compressor pressure ratio and the fuel flow rate in the burner [11]. A further step in the combined cycle power plant optimization was carried out by Ganjehkaviri et al. [12]. They proposed a multi-objective optimization based on the exergoeconomic and exergoenvironmental results. They increased the exergetic efficiency in 6%, while the cost rate of exergy destruction was reduced by less than 1%.

Besides traditional plant configurations, other works deal with innovative layouts to increase the plant performance. Ifaei et al. [13] replaced the conventional closed feedwater heaters of a Rankine cycle by natural draft wet cooling towers. A parametric study obtained an exergoeconomic optimum on a cogeneration system that included a gas turbine, a HRSG, a supercritical CO_2 (sCO_2) cycle and an organic Rankine cycle [14]. Other power plant designs integrated solar energy with a combined cycle and optimized the costs of exergy destruction by genetic algorithms [15] or multi-objective evolutionary algorithms [16]. An exergoeconomic analysis of a parabolic trough power plant studied the cooling options in the Rankine cycle showing the lowest exergy destruction in the wet cooling system [17]. Similarly, Elsafi [18] analyzed the non-reheating as well as steam–steam reheating configurations for a commercial-size direct steam generation parabolic trough solar thermal power plant. An optimum degree of reheating could maximize the exergetic efficiency, although no optimization point was found for the exergoeconomic results.

Solar power tower plants have been also analyzed based on exergy and economic approaches. A basic design of a SPTP with no energy storage system and a re-heated Rankine cycle showed that the maximum exergy loss occurs in the receiver system and the heliostats field [19]. The improvement of using a Kalina cycle, with water-ammonia as working fluid, rather than a Rankine cycle, is evaluated in [20]. The results showed that the two-tank of molten-salts storage system reduces the exergy destruction compared to a simple Rankine cycle. Soltani et al. [21] optimized a hybrid cogeneration cycle with a SPTP using a multi-objective approach focused on two functions: the exergetic efficiency and the total costs. Similarly, a parametric optimization of the exergetic efficiency using genetic algorithms was proposed by Wang and He [22]. They analyzed a molten salt SPTP integrated with a sCO_2 Brayton cycle showing that the optimum molten salt temperature would be 680 ºC. Kouta et al. [23] combined a SPTP with a sCO_2 Brayton cycle for power production and a multiple effect evaporation with thermal compression desalination system. They used the second law and the exergy analysis to determine the irreversibility production, which was maximum in the solar tower. Another exergetic and economic optimization of a SPTP with an open volumetric receiver hybridized with a cogeneration system is presented in [24]. However, no exergoeconomic approach was applied in these works. Only Toro et al. [25] performed an exergoeconomic analysis of a SPTP of 1.4 MW that employs air at 680 ºC as a heat transfer fluid in the receiver. The exergoeconomic results showed that neither the option of 1.5 hours of thermal storage nor a hybrid layout with a CH_4 combustion chamber present better performance than a conventional combined cycle.

The mentioned background reveals a deep interest in exergoeconomic analysis of power plants, the relevance of the HRSG in combined cycles and the interest of the steam generator (SG) design in SPTP on the overall plant behavior [10, 11]. In a SPTP, the SG is composed by preheater (PH), evaporator (EV), reheater (RH) and

190 superheater (SH) heat exchangers. One of the main variables for its design is the pinch
191 point temperature difference in the evaporator as it has a high impact on the heat
192 transfer areas of the SG, especially in the evaporator and the preheater [26]. González-
193 Gómez et al. [26] showed that the pinch point variation changes the thermal and
194 mechanical conditions of the heat exchangers of the SG, modifying the SG design and
195 costs. An optimum pinch point temperature of 2.5 ºC minimized the costs while fulfilled
196 the thermomechanical limitations of TEMA standards and Pressure Vessel code [27,
197 28]. Such optimization was carried out considering the SG, the operating costs of the
198 receiver and costs of the energy storage system. To the best of the authors'
199 knowledge, the performance of the optimum SG considering the entire power plant has
200 not been addressed yet.

201 In this work, the performance of a solar power tower plant is studied as a function of
202 the steam generator design applying exergy and exergoeconomic analyses.
203 The main variable used is the pinch point temperature difference in the evaporator,
204 which changes the plant operating conditions (salt mass flows, cold storage
205 temperature and pressure drops). The approach consists of designing a SG and a
206 storage system for each pinch point while the heliostats field, receiver and power block
207 designs are kept constant. The heat exchangers are designed accomplishing
208 thermomechanical limitations of TEMA standards [27] and ASME Pressure Vessel
209 code [28] using an economic optimization [26]. The results show the influence of the
210 SG on the plant performance obtaining an optimum pinch point to operate the plant that
211 minimizes the costs of exergy destruction.

212 **2. System description**

213 The solar power cycle analyzed is based on the design of Crescent Dunes with a water
214 cooled condenser [29]. This plant consists of a 110 MWe plant with 3.8 solar multiple
215 and 10 storage hours. The power cycle is a subcritical Rankine-cycle with regenerative
216 system and a steam generator that works with molten salt (60% $NaNO_3$ and 40%

KNO_3) absorbing the energy in the solar receiver. Water properties are calculated using CoolProp library [30] while molten salt properties are computed from [31, 32].

Figure 1 shows a detailed description of the plant, which is divided into solar field, storage system, steam generator (Fig. 1-a) and power block (Fig. 1-b). Pressure, temperature, mass flow and enthalpy data plotted in numeric values identify the unaltered values for the conditions considered.

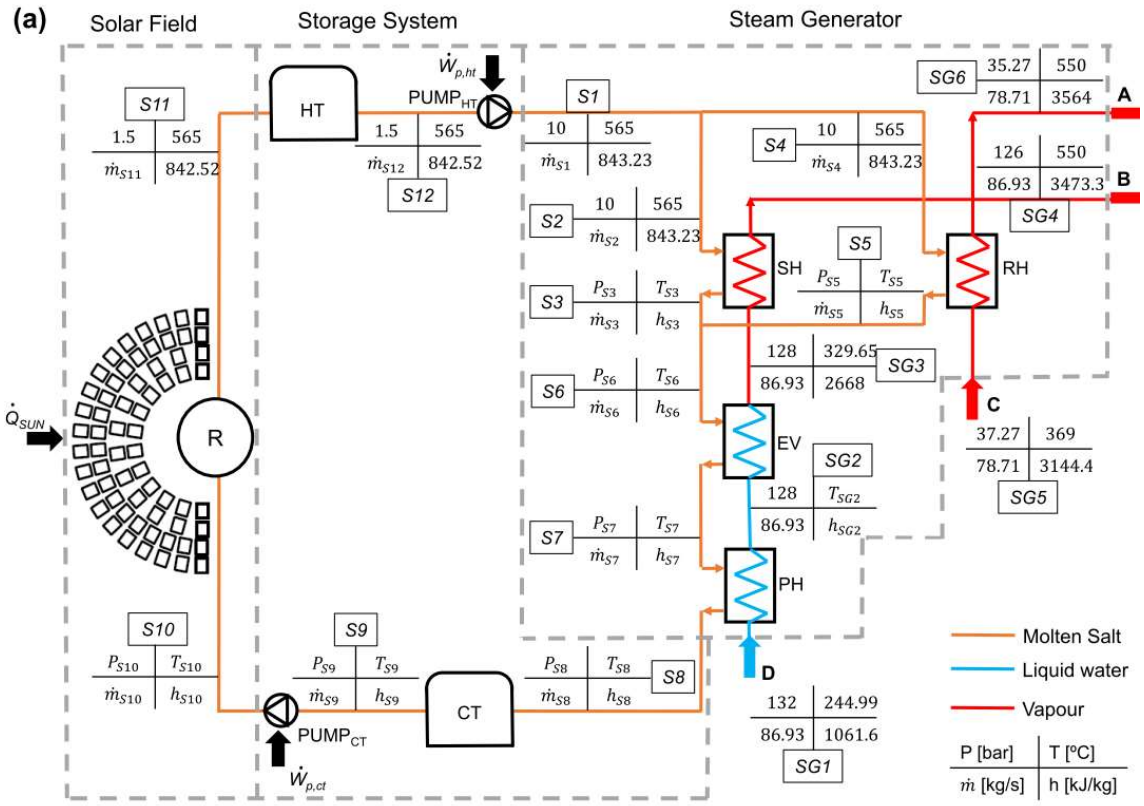

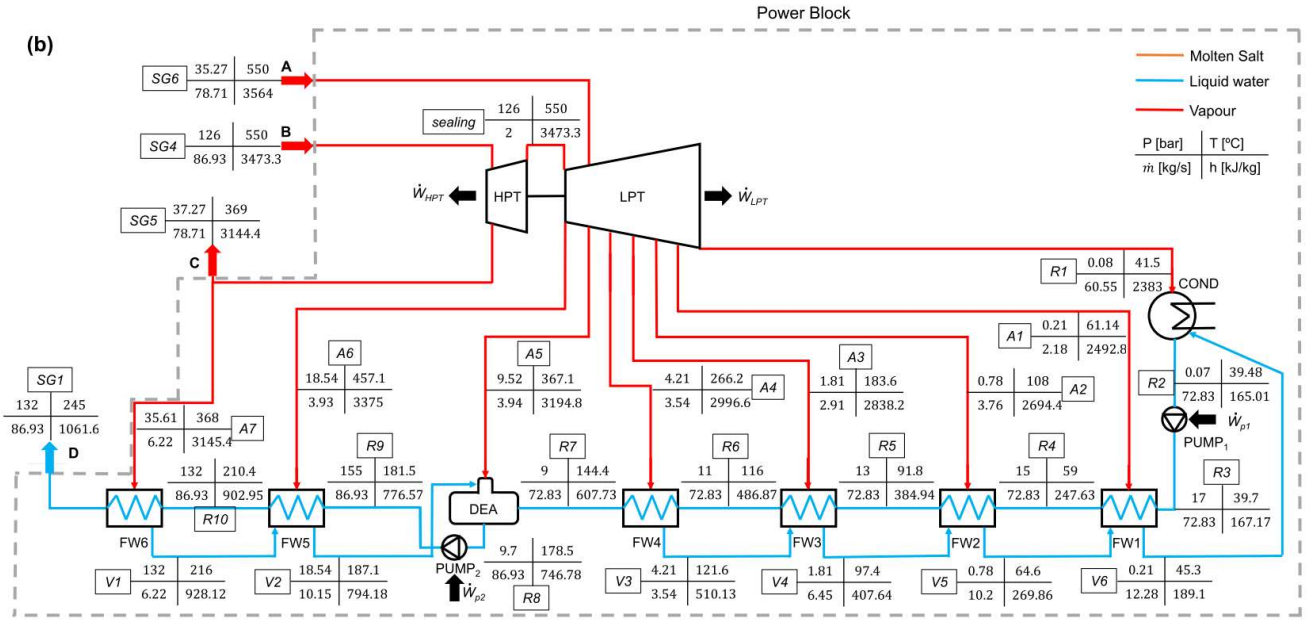

Figure 1. Schematic diagram of the solar power tower plant: (a) solar field, storage system and steam generator; (b) power block.

Regarding the solar part (Fig. 1-a), it comprises the heliostats field, which are arranged in radial configuration, the tower receiver, the two-storage tanks (one hot and one cold) and the molten salt pumps. Table 1 shows the main characteristics of these devices. The SG includes a train of heat exchangers: SH, RH, EV and PH, which transfer the energy stored in the hot tank to meet the energy requirements of the power block. Figure 2 shows the temperature profiles of the SG identifying the pinch point and the approach temperatures. Constant temperatures are plotted in black color while the calculated temperatures are plotted in red color. As can be seen, the solar system working conditions will change as a function of the pinch point temperature difference of the evaporator. The approach point is estimated ensuring non-steaming conditions on the PH, as it will be detailed in the following section.

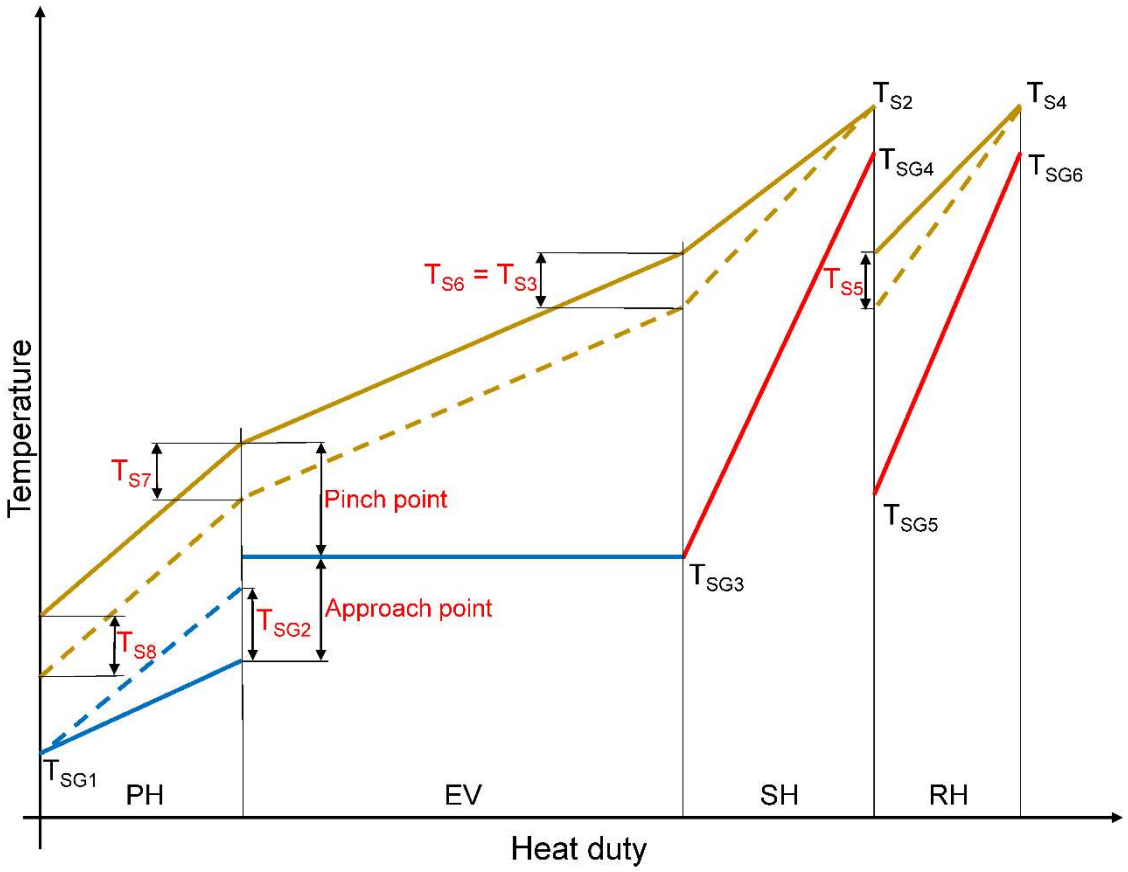

Figure 2. Temperature profiles for the SG. Salt temperatures profile in yellow line, water liquid in blue and water vapor in red lines. The text in black color identifies the fixed parameters, while red color identifies calculated temperatures.

The hot salt enters to the SG through the SH and RH at a constant temperature of T_{S2} = T_{S4} = 565 ºC, and leaves it through the PH at T_{S8}, which is equal to the temperature of the cold tank. As the power block works at 110 MWe independently of the pinch point temperature, the salt mass flow rate ($\dot{m}_{S1}$), the temperatures of the PH on the salt side (T_{S8} and T_{S7}) and on the water side (T_{SG2}), the temperatures of the salt on the EV (T_{S3} and T_{S7}) and the outlet temperature of the RH (T_{S5}) will change with the pinch point to fulfill the energy requirements of the power block (Figs. 1 and 2). Accordingly, costs, salt mass flows and pressure drops through each heat exchanger change as a function of the pinch point temperature difference. In general, as the pinch point increases, higher salt temperatures are obtained in the inlet of the PH and the cold storage tank, which increases the salt mass flow rate needed in the receiver.

To study the effect of the SG on the power plant, the pinch point temperature (PP_{EV}) is used as the main variable. This temperature difference varies from 1 to 10 ºC [26]. For each pinch point, a different SG is designed minimizing the overall costs while following the thermomechanical limitations of TEMA standards [27] and ASME Pressure Vessel code [28]. The design methodology is explained in the following section.

Table 1. Nominal values of the solar field, storage system and power block components [29, 33, 34].

Solar field and storage system		**Power block**	
Heliostats & Receiver		*Water pumps*	
Number of heliostats	10347	Pump 1 pressure increment ($\Delta P_{pump,1}$)	145.30 bar
Heliostat aperture area	115.7 m^2	Pump 1 efficiency ($\eta_{pump,1}$)	80.0 %
Tower height	195 m	Pump 2 pressure increment ($\Delta P_{pump,2}$)	16.93 bar
Receiver diameter	17.6 m	Pump 2 efficiency ($\eta_{pump,2}$)	85.6 %
Receiver size	20 m		
Emissivity of the receiver surface	0.85		
Storage system		*Condenser*	
Pump HT and CT efficiency	70 %	Condenser pressure (P_{R1})	0.0783 bar
Storage capacity	10 h	Inlet refrigerator temperature ($T_{ref,in}$)	20 ºC
Heat losses	1 %	Outlet refrigerator temperature ($T_{ref,out}$)	45 ºC

The power block provides a power of 110 MWe regardless of the pinch point value. To that end, pressure, temperature and mass flow of the steam in the inlet of the preheater (SG1), the inlet and outlet of the high pressure turbine (SG4 and SG5) and in the inlet of the low pressure turbine (SG6) are kept constant (Fig. 1-b, Fig. 2). These properties constraint the rest of working conditions of the power block. The power block comprises the condenser, two pumps, a deaerator and several feedwater heaters. The water stream is first preheated from $T_{SG1} = 250\ ºC$ and $P_{SG1} = 132\ bar$ and then heated

until superheating conditions ($T_{SG4} = 550\ ºC$ and $P_{SG4} = 126\ bar$). After expansion in the high pressure turbine (HPT), the water stream is reheated up to $T_{SG6} = 550\ ºC$ and $P_{SG6} = 35.27\ bar$ and expanded in the low pressure turbine (LPT). Table 1 shows the main characteristics of the power block components while Figure 3 represents the subcritical Rankine cycle in a T-s diagram for a pinch point of 10 ºC.

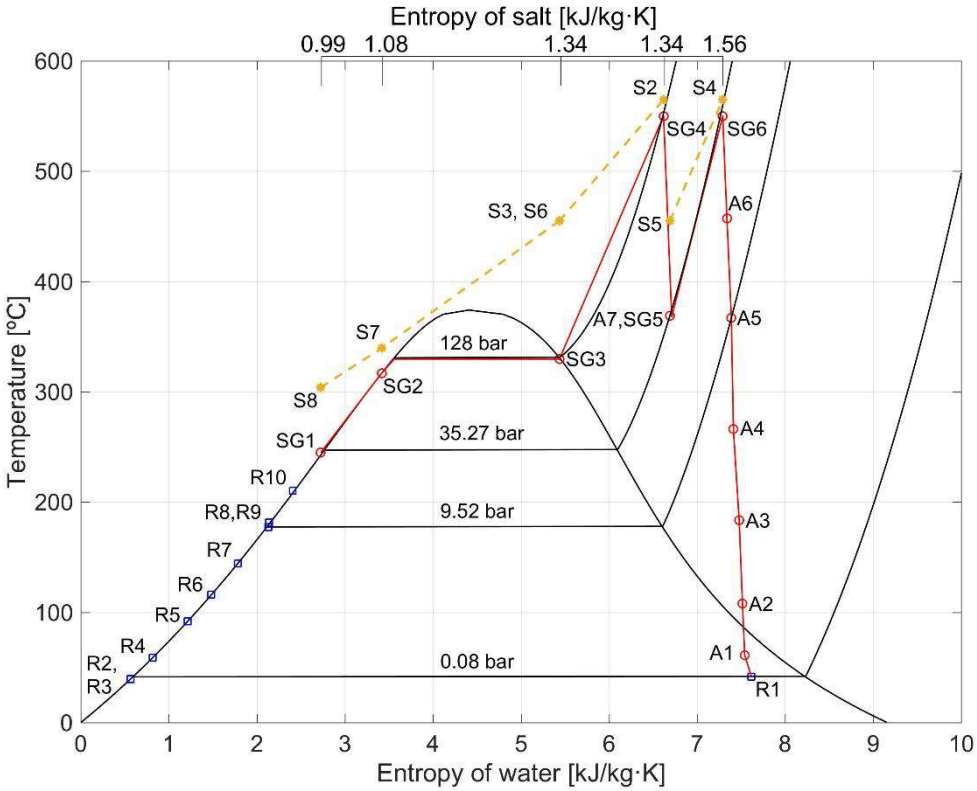

Figure 3. Temperature-Entropy diagram of the power cycle of water and molten salt with PP_{EV} = 10ºC. Notice that the upper salt entropy axis is not plotted at scale.

3. Mathematical model

This section describes the procedure followed to study the thermodynamic behavior of the power plant. Figure 4 shows a simplified scheme of the approach, which is further detailed in this section.

Firstly, pressure, temperature and mass flow values of the power block are estimated for a power of 110 MWe. Then, the values of pressure and temperature of the salt that

leaves the hot tank and the pressure of the evaporator are selected. Using these data and the properties of the heliostats field (Table 1), the energy fluxes on the receiver are calculated [35]. Later, a global economic optimization of the SG heat exchanger train (RH, SH, EV and PH) is carried out using GA and cost models for each pinch point [26]. Once the heat exchangers are designed accomplishing TEMA standards [27] and Pressure Vessel code [28], all mass flows, temperature and pressure values are know and can be used for the energy balance on each component. An exergy analysis is carried out to determine the exergy streams and the exergy destruction on each component. These results are employed as the input data for the exergoeconomic evaluation of the entire system for the different pinch points considered.

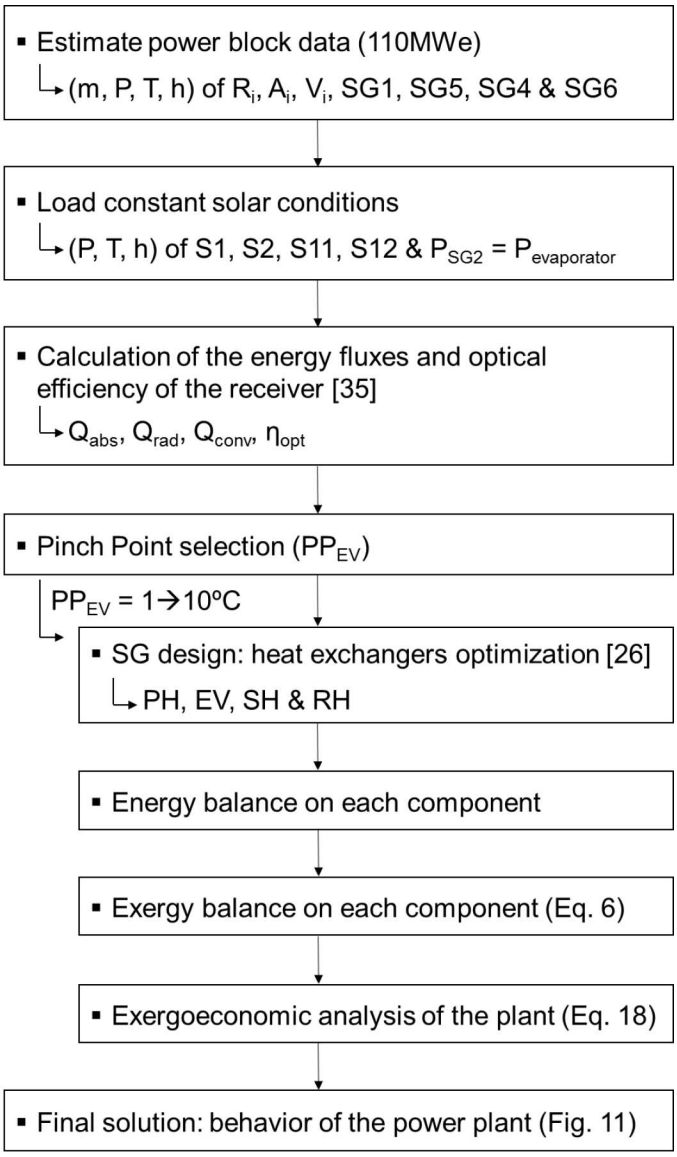

294 **Figure 4.** Schematic of the mathematical model.

295

296 **3.1. Steam generator design**

297 The steam generator design depends on the pinch point temperature difference (PP_{EV})
298 in the evaporator. The methodology used in this work follows the approach proposed
299 by González-Gómez et al. [26]. Each heat exchanger is designed according to TEMA
300 standards [27] and ASME Pressure Vessel code [28]. Material selection and technical
301 constraints are considered to assure the heat exchanger reliability [36]. Figure 5 shows
302 the scheme followed for the design of the SG for each pinch point analyzed.

303 First, the approach point is estimated for each pinch point. This temperature difference
304 between exit water of the economizer and the saturated water of the steam drum is
305 imposed to prevent subcooled flow boiling, i.e. generation of steam in the last part of
306 the economizer. As stated in [26], this approach temperature depends on the
307 manufacturers. In this work, the approach temperature is calculated minimizing the
308 total annualized cost (TAC) ensuring non-steaming conditions in the pre-heater.

309 A genetic algorithm is implemented to obtain a feasible and an economical design for
310 each heat exchanger. This optimization procedure ensures the implementation of the
311 technical constraints while handling the high number of variables that involve the heat
312 exchanger design [26] (Fig. 5). Thermomechanical limitations of TEMA standards [27]
313 and Pressure Vessel code [28] are considered.

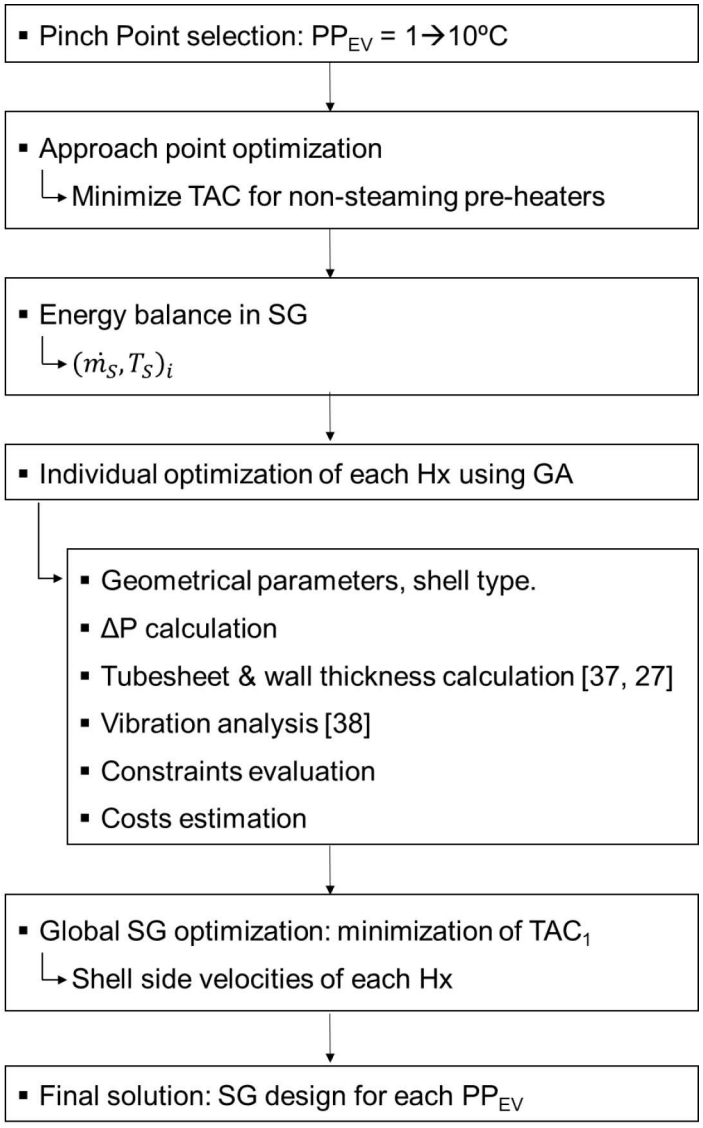

Figure 5. Schematic of the optimization algorithm.

Finally, the whole steam generator is optimized changing the velocity of the shell side of each heat exchanger. To that end, TAC_1 (Eq. 1) is minimized considering the capital costs ($C_{capital}$) of the heat exchangers, the operational pump cost (C_{pump}) and the start-up energy ($C_{start,SG}$) [26].

$$TAC_1 = frc \cdot C_{capital} + C_{operation} \quad (1)$$

$$C_{capital} = C_{Hx} + C_{pump} + C_{Tank} \quad (2)$$

$$C_{operation} = C_{pumping,R} + C_{pumping,SG} + C_{start,SG} \quad (3)$$

$$C_{pumping,i} = c_{power} \frac{H_{opd,i}}{\eta_{pump}} \left(\frac{\dot{m}_i \Delta P_i}{\rho_i} \right) \quad (4)$$

$$C_{start,SG} = c_{power} \left[\sum_{j=1}^{M} V_j \rho_j \left(N_{hot} \Delta h_{j,hot} + N_{warm} \Delta h_{j,warm} \right) + W_{hx} Cp_w (N_{hot} \Delta T_{hot} + N_{warm} \Delta T_{warm}) \right] \eta_{PB} \quad (5)$$

The energy electricity cost (c_{power}) is assumed as 0.13 €/kWhe, the pump efficiency (η_{pump}) was described in Table 1, the number of hot start-ups (N_{hot}) and warm start-ups (N_{warm}) are 300 and 10 [26], respectively; and the operating time of each component is described in the following section.

3.2 Exergy analysis

The SPTP is analyzed performing energy and exergy balances. For the exergy balance, it is necessary to define the properties of the dead state as the maximum work depends on its definition. The influence of the dead state on the exergy analysis of power plants has been analyzed in [9, 39-41]. In general, the dead state temperature has a low influence on the main results of the exergy analysis, decreasing slightly the exergy efficiency of the plant as the environment temperature increases [9]. In this study, a fixed dead state defined by $T_0 = 20ºC$ and $P_0 = 1\ bar$ is used for both water and molten salts.

The exergy balance applied to each component, *k*, considering a control volume in steady state can be expressed as:

$$\sum_i^N \left(1 - \frac{T_0}{T_i}\right) \cdot \dot{Q}_{i,k} + \sum_i^N \dot{E}_{i,k} = \dot{E}_{W,k} + \sum_e^N \dot{E}_{e,k} + \dot{E}_{D,k} \quad (6)$$

where the first term is related to the exergy produced by a heat energy transfer $\dot{Q}$ through the boundary of the control volume at a temperature of T_i, $\dot{E}_i$ and $\dot{E}_e$ refer to the exergy of the inlet and outlet streams respectively, $\dot{E}_W$ refers to the exergy transferred as work, and $\dot{E}_D$ is the exergy destruction rate in the component.

The general expression of the exergy transfer rate at control volume inlets and outlets is written as:

$$\dot{E} = \dot{E}_{ph} + \dot{E}_{ch} = \dot{m}\left[(h - h_0) - T_0(s - s_0) + \frac{1}{2}V^2 + gz + e^{CH}\right] \qquad (7)$$

where the exergy rate depends on the physical ($\dot{E}_{ph}$) and chemical ($\dot{E}_{ch}$) components. In the present work, the composition of the working fluids, molten salt and water, remain unaltered, consequently, no chemical changes are considered. Kinetic and potential exergies are neglected.

The exergy balance of each component can be carried out applying Eq. (6) or using the approach developed by Lozano and Valero [42]. This method classifies the exergy flows for each component in fuel, product or loss (F-P-L). The product represents the desired result produced by the system, while the fuel accounts the exergy flow needed for each component. The difference between the fuel and the product is the exergy destructed, or lost, by the system, Eq. 8. Table 2 shows the fuel and product definitions of each component.

$$\dot{E}_D = \dot{E}_{FUEL} - \dot{E}_{PRODUCT} \qquad (8)$$

Following the F-P-L definition, the exergy efficiency of each component can be expressed as:

$$\varepsilon = \frac{\dot{E}_{PRODUCT}}{\dot{E}_{FUEL}} \qquad (9)$$

Table 2. Fuel-product exergy definitions for components.

	Component	Fuel	Product
SF+R	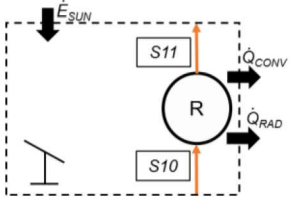	$\dot{E}_{SUN} - \left(1 - \frac{T_0}{T_R}\right) \cdot \dot{Q}_{rad} - \left(1 - \frac{T_0}{T_R}\right) \cdot \dot{Q}_{conv}$	$\dot{E}_{S11} - \dot{E}_{S10}$
$Pump_{HT}$, $Pump_{CT}$, $PUMP_1$, $PUMP_2$	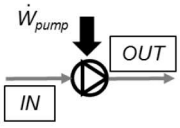	$\dot{W}_{pump}$	$\dot{E}_{OUT} - \dot{E}_{IN}$
SH, EV, PH, RH	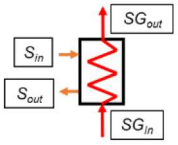	$\dot{E}_{S_{in}} - \dot{E}_{S_{out}}$	$\dot{E}_{SG_{out}} - \dot{E}_{SG_{in}}$
$TES_{HT,CT}$	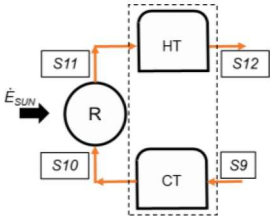	*Eq. (16)	
HPT	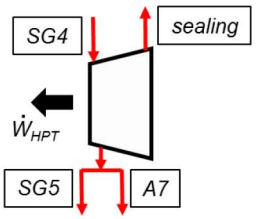	$\dot{E}_{SG4} - \dot{E}_{SG5} - \dot{E}_{A7} - \dot{E}_{sealing}$	$\dot{W}_{HPT}$
LPT	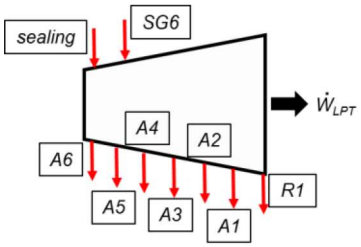	$\dot{E}_{SG6} + \dot{E}_{sealing} - \dot{E}_{A6} - \dot{E}_{A5} - \dot{E}_{A4} - \dot{E}_{A3} - \dot{E}_{A2} - \dot{E}_{A1} - \dot{E}_{R1}$	$\dot{W}_{HPT}$
COND	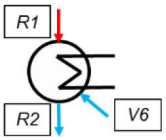	$\dot{E}_{R2} - \dot{E}_{R1} - \dot{E}_{V6}$	$\dot{E}_{ref,out} - \dot{E}_{ref,in}$

FW1, FW2, FW3, FW5	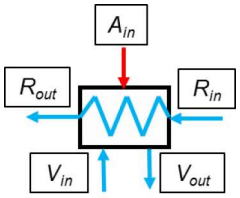	$\dot{E}_{A_{in}} + \dot{E}_{V_{in}} - \dot{E}_{V_{out}}$	$\dot{E}_{R_{out}} - \dot{E}_{R_{in}}$
FW4, FW6	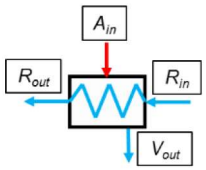	$\dot{E}_{A_{in}} - \dot{E}_{V_{out}}$	$\dot{E}_{R_{out}} - \dot{E}_{R_{in}}$
DEA	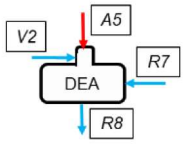	$\dot{E}_{A5} + \dot{E}_{V2'} + \dot{E}_{R7}$	$\dot{E}_{R8}$

368

369 The solar tower and the solar field are considered as a single device (the receiver) that
370 receives the exergy flux of the solar radiation. Following the exergy balance and
371 correlation developed by Petela [43, 44]:

372 $$\dot{E}_{FUEL,R} = \dot{E}_{SUN} - \left(1 - \frac{T_0}{T_R}\right)\dot{Q}_{rad} - \left(1 - \frac{T_0}{T_R}\right)\dot{Q}_{conv} \quad (10)$$

373 $$\dot{E}_{SUN} = \dot{Q}_{SUN} \cdot \left(1 - \frac{4}{3}\frac{T_0}{T_S} + \frac{1}{3}\frac{{T_0}^4}{{T_S}^4}\right) \quad (11)$$

374 where $T_S = 5770\ K$ is the Sun temperature, T_R is the receiver surface temperature and
375 $\dot{Q}_{SUN}$ is the power supplied by the Sun. Such an energy computes the energy absorbed
376 by the molten salt ($\dot{Q}_{abs}$) and the heat losses by radiation and convection ($\dot{Q}_{rad}$ and
377 $\dot{Q}_{conv}$ respectively) and the optical efficiency of the field of heliostats (η_{opt}):

378 $$\dot{Q}_{SUN} = \frac{\dot{Q}_{incident}}{\eta_{opt}} = \frac{\dot{Q}_{abs} + \dot{Q}_{rad} + \dot{Q}_{conv}}{\eta_{opt}} \quad (12)$$

379 $$\dot{Q}_{rad} = \varepsilon_e \sigma A_R F_{view}\left({T_R}^4 - {T_0}^4\right) \quad (13)$$

380 $$\dot{Q}_{conv} = h A_R (T_R - T_0) \quad (14)$$

where $\varepsilon_e = 0.85$ is the receiver thermal emittance, $\sigma = 5.67 \cdot 10^{-8}\ W/m^2K$ is the Stefan-Boltzmann constant, F_{view} is the radiative view factor from the receiver surface to the surroundings that is equal to 1 as a conservative selection, A_R is the receiver surface and h is the convective heat transfer coefficient [33]. The methodology described by Rodriguez-Sanchez et al. [35] has been used to compute: $\dot{Q}_{abs}$, $\dot{Q}_{rad}$, $\dot{Q}_{conv}$, η_{opt} and the incident energy ($\dot{Q}_{incident}$) reflected from the heliostats to the tower. These parameters have been calculated for the 21st of March, which is considered as a representative day for the entire year. The operation mode of the plant is studied applying an energy and exergy analyses in order to reflect hourly the evolution of the exergy destruction rate of each component, following the approach described in [43].

Figure 6 shows the evolution of energy and exergy fluxes for the day modelled. The energy absorbed in the receiver varies hourly while the energy needed to operate the power block is constant. Once there is enough energy accumulated in the tanks, it is possible to start producing 110 MWe. The energy absorbed throughout the day enables the power block operation during 11.94 hours per day, which is initiated at 10 AM. The exergy of the Sun, the exergy destruction rate of the heliostats and the receiver, and the exergy destruction rate of the power block are shown in dotted lines in Fig. 6. These results are obtained using Table 2. As the exergy destruction rate is used in the exergoeconomic analysis, it is necessary to obtain a daily averaged value that considers the variations presented in Fig. 6. Therefore, the exergy destruction rate of the components is averaged considering the operating hours of the receiver (8 hours), TES (10 hours), SG (11.94 h) and power block components (11.94 h) per day.

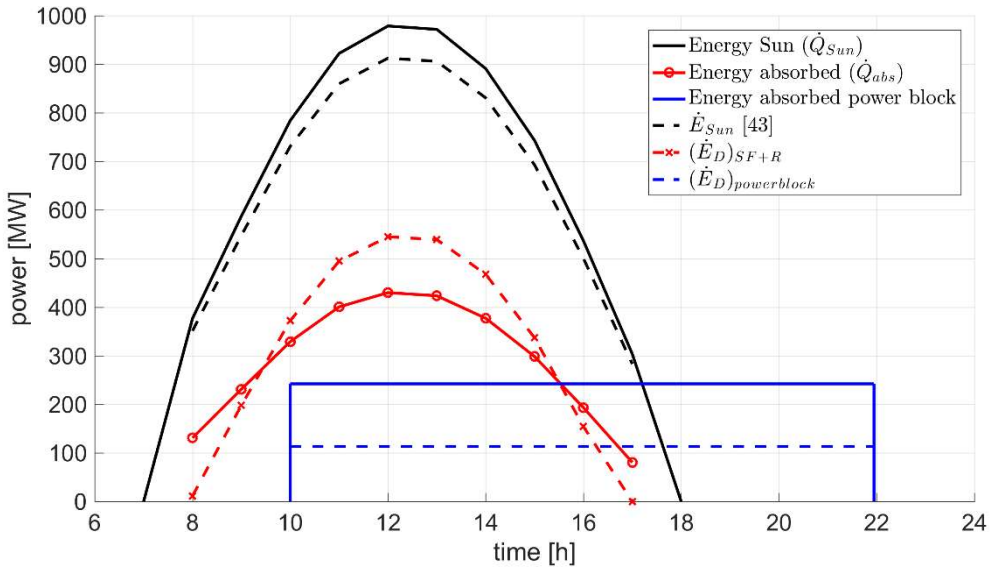

403

404 **Figure 6.** Operation mode analysis (21st of March): energy and exergy results

405 considering the receiver and the power block components.

406 The exergy balances shown in Table 4 are estimated at steady conditions for all

407 devices in the power cycle in which there is no mass or energy storage. However, the

408 two-tank thermal storage system works storing energy and exergy during the charging

409 and discharging processes in a non-stationary process [23, 45, 47]. To consider such

410 behavior and the rest of components of the entire plant, it is necessary to average the

411 exergy destructed of the two-tank energy storage system. The analysis considers both

412 tanks in an averaged daily operation, the operation time of the charging process is the

413 same hours as the tower receptor (8 hours per day) while the discharging process is

414 designed to work at full load conditions during 10 hours per day. Furthermore, the

415 modeling of the two-tank thermal storage is carried out assuming 1% of heat losses

416 (Table 1) [34]. Following the approach shown in [48], the energy and exergy balances

417 of the TES system analyze the operation of both cold and hot tanks for a daily

418 operation:

$$\int_0^{24}([\dot{m}_{S11}(h_{S11}-h_{S10})]_{CHARGE}+[\dot{m}_{S11}(h_{S11}-h_{S10})]_{DISCHARGE})dt$$

$$=\int_0^{24}([\dot{m}_{S1}(h_{S1}-h_{S8})]_{CHARGE}+[\dot{m}_{S1}(h_{S1}-h_{S8})]_{DISCHARGE})dt$$

$$+\bar{Q}_{LOSS,TES}$$

(15)

$$\int_0^{24}\left(\left[\dot{E}_{S11}-\dot{E}_{S10}\right]_{CHARGE}+\left[\dot{E}_{S11}-\dot{E}_{S10}\right]_{DISCHARGE}\right)dt$$

$$=\int_0^{24}\left(\left[\dot{E}_{S1}-\dot{E}_{S8}\right]_{CHARGE}+\left[\dot{E}_{S1}-\dot{E}_{S8}\right]_{DISCHARGE}\right)dt$$

$$+\left(1-\frac{T_0}{T_{HT}}\right)\bar{Q}_{LOSS,TES}+\bar{E}_{D,TES}$$

(16)

where $\bar{Q}_{LOSS,TES}$ represents the daily-averaged heat losses and $\bar{E}_{D,TES}$ the daily-averaged exergy destruction in both tanks. Note that the exergy flow due to the heat losses is estimated assuming that the system is at the hot tank temperature, which is a conservative consideration.

Regarding the HPT and LPT turbines, an extraction from the HPT is used to seal the LPT turbine in order to avoid the bypass or leakages of the steam, as pointed in Fig. 1-b. Furthermore, exergetic efficiency of the plant can be expressed as:

$$\varepsilon_{CYCLE}=\frac{\dot{W}_{NET}}{\dot{E}_{SUN}} \qquad (17)$$

where $\dot{W}_{NET}$ is the net power of the plant.

3.3 Exergoeconomic analysis

The thermoeconomic studies combine exergy analysis and economic principles to provide valuable information about the design and operation of a system. In this analysis, the minimization of the total cost rate ensures the plant optimization. Several

studies have been proposed for the exergoeconomic study of a system [1, 2, 4, 5, 42, 47]. In this work, the specific exergy costing method (SPECO) is employed [48]. This approach consists of evaluating each component using a cost balance, in which all energy and exergy values of the inlet and outlet streams are accounted. This balance, combined with appropriate auxiliary thermoeconomic relations, results in a system of linear algebraic equations that is solved for the unknown values of cost rates or cost per exergy unit. The procedure classifies the costs in fuel and product, which are similarly defined and obtained as in the previous section.

For a system operating at steady state considering entering and exiting streams as well as both heat and work interactions with the surroundings, the cost balance equation for the *k*th component becomes:

$$\sum_e^N \dot{C}_{e,k} + c_{w,k}\dot{W}_k = c_{q,k}\dot{Q}_k + \sum_i^N \dot{C}_{i,k} + \dot{Z}_k \qquad (18)$$

where the costs of the inlet and outlet streams, $\dot{C}_i$ and $\dot{C}_e$ respectively, are defined as the product of the cost per exergy unit *c*:

$$\dot{C} = c\dot{E} \qquad (19)$$

The term $\dot{Z}$ in Eq. 18 is the cost rate related to the capital investment and the operating and maintenance costs: $\dot{Z}_k = \dot{Z}_k^{CI} + \dot{Z}_k^{OM}$ [1]. The operating costs ($\dot{Z}_k^{OM}$) of pumping are estimated using Eq. 4. Regarding the capital investment costs, the purchasing cost unit (*PUC*) can be converted into cost per unit time using the annuity factor (f_{ann}) and the annual number of operation hours (H_{opd}):

$$\dot{Z}_k^{CI} = \frac{PUC_k \cdot f_{ann} \cdot \varphi}{H_{opd}} \qquad (20)$$

where $\varphi = 1.06$ is the maintenance factor. The annuity factor can be estimated as:

$$f_{ann} = \left[\frac{q^{lf+cp}-1}{(q-1)q^{lf+cp}} - \frac{q^{cp}-1}{(q-1)q^{cp}}\right]^{-1} \qquad (21)$$

$$q = \left(1 + \frac{in}{100}\right)\left(1 + \frac{ri}{100}\right) \qquad (22)$$

where *in* and *ri* are the interest rate and the rate of inflation respectively, *lf* accounts the lifetime of the plant and *cp* the construction period [15, 18]. The economic approach shown in Gónzalez-Gómez et al. [26] is employed. A simplified economic model is used assuming a lifetime of $lf = 25$ years with and interest rate of *in* = 8% and neglecting the inflation and the construction period. Considering a year with the modeled day analyzed in Fig. 6, the operation time of the power block, the SG and the high temperature pump is H_{opd} = 4360 h while the operation time of the cold temperature pump and the receiver is H_{opd} = 2920 h. The two-tank energy storage costs are estimated using NREL results [34] and the costs estimation approach proposed in [49]. Similarly, the capital cost of the SG heat exchangers (and the salt pumps are estimated using Purohit method [50], as was described by González-Gómez et al. [26]. The purchasing unit cost of the receiver (PUC_R) and the heliostats field (PUC_{SF}) is estimated following NREL results [51]:

$$PUC_{SF+R} = PUC_{SF} + PUC_R = 355A_{aperture} + (1835.7h_R - 25868h_R + 3 \cdot 10^7) \qquad (23)$$

where $A_{aperture}$ is the aperture area of the solar field and h_R is the height of the solar tower. As the pinch point is changing, the capital investment costs of the steam generator and storage system are modified while the receiver and heliostats costs remain constant. Regarding the capital investments of the power block, Table 4 describes the correlations employed:

Table 3. Economic estimations for the power plant components [8, 9, 18].

Component	Purchasing unit cost [$]	Comments
Steam Turbine	$PUC = 6000\left(\dot{W}_{turbine}\right)^{0.7}$	$\dot{W}_{turbine}$ is the power of the turbine [kW]
Water pumps	$PUC = 1773\left(\dot{W}_{PUMP}\right)^{0.7}$	$\dot{W}_{PUMP}$ is the power of the pump [kW]

Feed water heaters	$PUC = 66 \cdot \dot{Q}\left(\frac{1}{T_{TTD} + a_3}\right)^{0.1}$	$\dot{Q}$ is the heat transferred [kW] T_{TTD} is the temperature difference between the saturated extraction steam and the feedwater outlet temperature $a_3 = 4$ for low pressure feed water heaters and $a_3 = 6$ for high pressure feed water heaters
Deaerator	$PUC = 145315(\dot{m}_{DEA})^{0.7}$	$\dot{m}_{DEA}$ is the mass flow through the deaerator
Condenser	$PUC = 1773 \cdot \dot{m}_{COND}$	$\dot{m}_{COND}$ is the mass flow of saturated water through the condenser

484

485 In order to perform the thermoeconomic evaluation of the power system, it is necessary
486 to apply the cost balance equation (Eq. 18) to each component obtaining a system of
487 equations. As stated in [1], depending on the number of streams entering and exiting
488 the component, some auxiliary equations are needed. Table 4 shows the cost rate
489 balance equation and the auxiliary equations for each device. Note that the cooling
490 water and the sun energy are considered as a free source and its cost rate is
491 neglected.

492 **Table 4**. Exergy cost rate balance and auxiliary equations for system components.

Component	Exergetic cost rate balance equation	Auxiliary equation
SF+R	$\dot{C}_{S11} = \dot{C}_{S10} + \dot{C}_{SUN} + \dot{Z}_{SF+R}$	$\dot{C}_{SUN} = 0$
$Tank_{HT}$	$\dot{C}_{S12} = \dot{C}_{S11} + \dot{Z}_{TES_{HT}}$	nil
$PUMP_{HT}$	$\dot{C}_{S1} - \dot{C}_{Wpump_{HT}} = \dot{C}_{S12} + \dot{Z}_{pump_{HT}}$	$\frac{\dot{C}_{pump_{HT}}}{\dot{W}_{pump_{HT}}} = \frac{\dot{C}_{pump_1}}{\dot{W}_{pump_1}}$

Separation point	$\dot{C}_{S2} + \dot{C}_{S4} = \dot{C}_{S1}$	$\frac{\dot{C}_{S2}}{\dot{E}_{S2}} = \frac{\dot{C}_{S4}}{\dot{E}_{S4}}$
SH	$\dot{C}_{S3} + \dot{C}_{SG4} = \dot{C}_{S2} + \dot{C}_{SG3} + \dot{Z}_{SH}$	$\frac{\dot{C}_{S2}}{\dot{E}_{S2}} = \frac{\dot{C}_{S3}}{\dot{E}_{S3}}$
Mixing point	$\dot{C}_{S6} = \dot{C}_{S3} + \dot{C}_{S5}$	nil
EV	$\dot{C}_{S7} + \dot{C}_{SG3} = \dot{C}_{S6} + \dot{C}_{SG2} + \dot{Z}_{EV}$	$\frac{\dot{C}_{S6}}{\dot{E}_{S6}} = \frac{\dot{C}_{S7}}{\dot{E}_{S7}}$
PH	$\dot{C}_{S8} + \dot{C}_{SG2} = \dot{C}_{S7} + \dot{C}_{SG1} + \dot{Z}_{PH}$	$\frac{\dot{C}_{S7}}{\dot{E}_{S7}} = \frac{\dot{C}_{S8}}{\dot{E}_{S8}}$
RH	$\dot{C}_{S5} + \dot{C}_{SG6} = \dot{C}_{S4} + \dot{C}_{SG5} + \dot{Z}_{PH}$	$\frac{\dot{C}_{S4}}{\dot{E}_{S4}} = \frac{\dot{C}_{S5}}{\dot{E}_{S5}}$
Tank_{CT}	$\dot{C}_{S9} = \dot{C}_{S8} + \dot{Z}_{TES_{CT}}$	nil
PUMP_{CT}	$\dot{C}_{S10} - \dot{C}_{Wpump_{CT}} = \dot{C}_{S9} + \dot{Z}_{pump_{CT}}$	$\frac{\dot{C}_{pump_{CT}}}{\dot{W}_{pump_{CT}}} = \frac{\dot{C}_{pump_1}}{\dot{W}_{pump_1}}$
HPT	$\dot{C}_{SG5} + \dot{C}_{A7} + \dot{C}_{seal} + \dot{C}_{W_{HPT}} = \dot{C}_{SG4} + \dot{Z}_{HPT}$	$\frac{\dot{C}_{HPT}}{\dot{W}_{HPT}} = \frac{\dot{C}_{LPT}}{\dot{W}_{LPT}}; \frac{\dot{C}_{SG4}}{\dot{E}_{SG4}} = \frac{\dot{C}_{A7}}{\dot{E}_{A7}}; \frac{\dot{C}_{SG4}}{\dot{E}_{SG4}} = \frac{\dot{C}_{SG5}}{\dot{E}_{SG5}}$
LPT	$\dot{C}_{R1} + \dot{C}_{A1} + \dot{C}_{A2} + \dot{C}_{A3} + \dot{C}_{A4} + \dot{C}_{A5} + \dot{C}_{A6} + \dot{C}_{W_{LPT}} = \dot{C}_{SG6} + \dot{C}_{seal} + \dot{Z}_{LPT}$	$\frac{\dot{C}_{SG6}}{\dot{E}_{SG6}} = \frac{\dot{C}_{R1}}{\dot{E}_{R1}}; \frac{\dot{C}_{SG6}}{\dot{E}_{SG6}} = \frac{\dot{C}_{A1}}{\dot{E}_{A1}}; \frac{\dot{C}_{SG6}}{\dot{E}_{SG6}} = \frac{\dot{C}_{A2}}{\dot{E}_{A2}}; \frac{\dot{C}_{SG6}}{\dot{E}_{SG6}} = \frac{\dot{C}_{A3}}{\dot{E}_{A3}}; \frac{\dot{C}_{SG6}}{\dot{E}_{SG6}} = \frac{\dot{C}_{A4}}{\dot{E}_{A4}}; \frac{\dot{C}_{SG6}}{\dot{E}_{SG6}} = \frac{\dot{C}_{A5}}{\dot{E}_{A5}}; \frac{\dot{C}_{SG6}}{\dot{E}_{SG6}} = \frac{\dot{C}_{A6}}{\dot{E}_{A6}}$
COND	$\dot{C}_{R2} + \dot{C}_{ref_{OUT}} = \dot{C}_{R1} + \dot{C}_{ref_{IN}} + \dot{C}_{V6} + \dot{Z}_{COND}$	$\dot{C}_{ref_{IN}} = 0; \frac{\dot{C}_{R1}}{\dot{E}_{R1}} = \frac{\dot{C}_{R2}}{\dot{E}_{R2}}$
PUMP_1	$\dot{C}_{R3} - \dot{C}_{Wpump_1} = \dot{C}_{R2} + \dot{Z}_{pump_1}$	$\frac{\dot{C}_{pump_1}}{\dot{W}_{pump_1}} = \frac{\dot{C}_{HPT}}{\dot{W}_{HPT}}$

FW1	$\dot{C}_{R4} + \dot{C}_{V6} = \dot{C}_{R3} + \dot{C}_{V5'} + \dot{C}_{A1} + \dot{Z}_{fw1}$	$\frac{\dot{C}_{A1}}{\dot{E}_{A1}} = \frac{\dot{C}_{V6}}{\dot{E}_{V6}}$
FW2	$\dot{C}_{R5} + \dot{C}_{V5} = \dot{C}_{R4} + \dot{C}_{V4'} + \dot{C}_{A2} + \dot{Z}_{fw2}$	$\frac{\dot{C}_{A2}}{\dot{E}_{A2}} = \frac{\dot{C}_{V5}}{\dot{E}_{V5}}$
FW3	$\dot{C}_{R6} + \dot{C}_{V4} = \dot{C}_{R5} + \dot{C}_{V3'} + \dot{C}_{A3} + \dot{Z}_{fw3}$	$\frac{\dot{C}_{A3}}{\dot{E}_{A3}} = \frac{\dot{C}_{V4}}{\dot{E}_{V4}}$
FW4	$\dot{C}_{R7} + \dot{C}_{V3} = \dot{C}_{R6} + \dot{C}_{A4} + \dot{Z}_{fw4}$	$\frac{\dot{C}_{A4}}{\dot{E}_{A4}} = \frac{\dot{C}_{V3}}{\dot{E}_{V3}}$
DEA	$\dot{C}_{R8} = \dot{C}_{R7} + \dot{C}_{V2'} + \dot{C}_{A5} + \dot{Z}_{dea}$	nil
$PUMP_2$	$\dot{C}_{R9} - \dot{C}_{Wpump_2} = \dot{C}_{R8} + \dot{Z}_{pump_2}$	$\frac{\dot{C}_{pump_2}}{\dot{W}_{pump_2}} = \frac{\dot{C}_{pump_1}}{\dot{W}_{pump_1}}$
FW5	$\dot{C}_{R10} + \dot{C}_{V2} = \dot{C}_{R9} + \dot{C}_{V1'} + \dot{C}_{A6} + \dot{Z}_{fw5}$	$\frac{\dot{C}_{A6}}{\dot{E}_{A6}} = \frac{\dot{C}_{V2}}{\dot{E}_{V2}}$
FW6	$\dot{C}_{SG1} + \dot{C}_{V1} = \dot{C}_{R10} + \dot{C}_{A7} + \dot{Z}_{fw6}$	$\frac{\dot{C}_{A7}}{\dot{E}_{A7}} = \frac{\dot{C}_{V1}}{\dot{E}_{V1}}$

Once the linear system of equations is solved, the exergy cost of each stream ($\dot{C}$) is used to obtain the cost per unit exergy of fuel ($c_{F,k}$) and product ($c_{P,k}$). The exergoeconomic behavior of the system is evaluated calculating the cost rate of exergy destruction ($\dot{C}_{D,k}$), the exergoeconomic factor (f_k) and the total cost rate ($\dot{C}_{total}$):

$$c_{F,k} = \dot{C}_{F,k}/\dot{E}_{F,k} \quad (24)$$

$$c_{P,k} = \dot{C}_{P,k}/\dot{E}_{P,k} \quad (25)$$

$$\dot{C}_{D,k} = c_{F,k}\dot{E}_{D,k} \quad (26)$$

$$f_k = \dot{Z}_k/\left(\dot{Z}_k + \dot{C}_{D,k}\right) \quad (27)$$

$$\dot{C}_{total} = \sum_k^N \dot{Z}_k + \sum_k^N \dot{C}_{D,k} \quad (28)$$

5. Results and discussion

First, the SG design for each pinch point is presented. Later, energy and exergy balances are applied to each component to solve the exergoeconomic model of the power plant.

5.1 Steam generator design

The high temperature differences between the inlet and the outlet of the working fluids produce different thermal expansion in the shell and the tubes of heat exchangers. To deal with this issue, U-tube heat exchangers are selected [26]. A common configuration is proposed for all pinch points: counter-current U-shell/U-tube heat exchangers design is used for RH and SH, while a straight shell U-tube is proposed for PH and EV.

The SG design process described in Fig. 5 determines the SG design. Geometric dimensions and selected materials of the heat exchangers are detailed in [26]. Focusing on the evolution of the costs as a function of the pinch point, on the one hand, low pinch point values may obtain large heat transfer areas, and thus, high capital costs and high energy consumption during the start-up. On the other hand, high pinch point values may increase the operational costs since a higher mass flow is needed, increasing also the storage tank size. Figure 7 presents the annualized cost for the capital investment of the heat exchangers and the operating and maintenance costs of the salt pumps. There is a clear influence of the pinch point on the PH and the EV, reducing its costs as the pinch point increases [26]. However, the high salt mass flow of cold salt leads to higher operating costs of the cold pump.

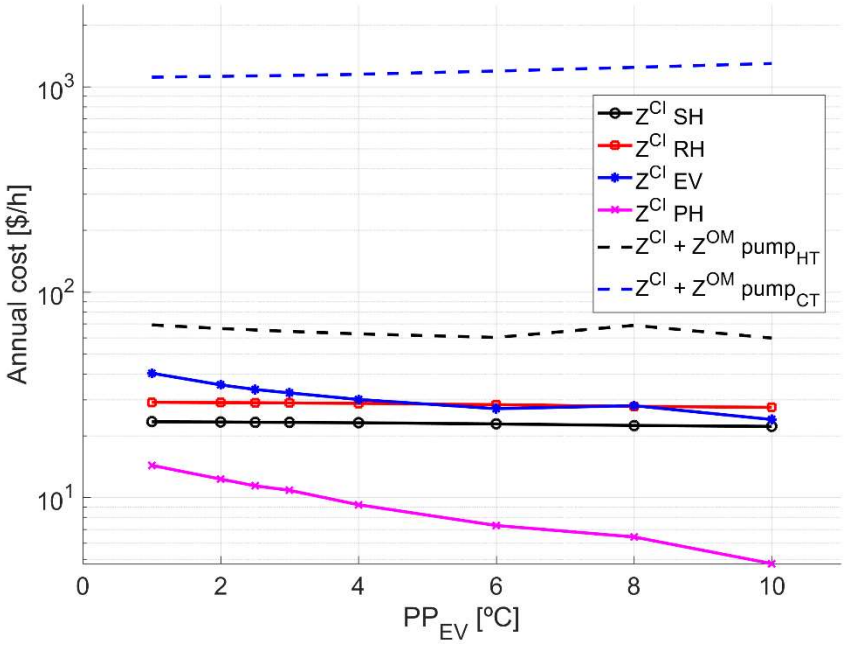

525

526 **Figure 7**. Evolution of different capital investment (CI) and operating and maintenance
527 (OM) costs in logarithmic scale against the pinch point.

528 **5.2 Exergy and exergoeconomic results**

529 The exergy destructed by each component is plotted in logarithmic axis in Fig. 8-a
530 sorted in descending order for the pinch points analyzed. Fig. 8-b shows the difference
531 between the exergy results of each pinch point and PP_{EV} = 1 ºC in order to analyze its
532 variation.

533 Most of the exergy is destructed in the heliostats field and receptor, followed by the
534 condenser and the energy storage system (Fig. 8-a). This is due to the high heat fluxes
535 on these devices. Similar results have been reported in the literature [19]. Lower
536 exergy destruction values are obtained for the low pressure turbine, which is higher
537 than the exergy destructed in the HPT due to the higher amount of steam extractions
538 from de LPW that increases the entropy generated. It is worth to note the high exergy
539 destruction values in the cold salt pump and the water pump 2 due to their high
540 pressure drops. Finally, DEA and all feedwater heaters show low exergy destruction
541 values.

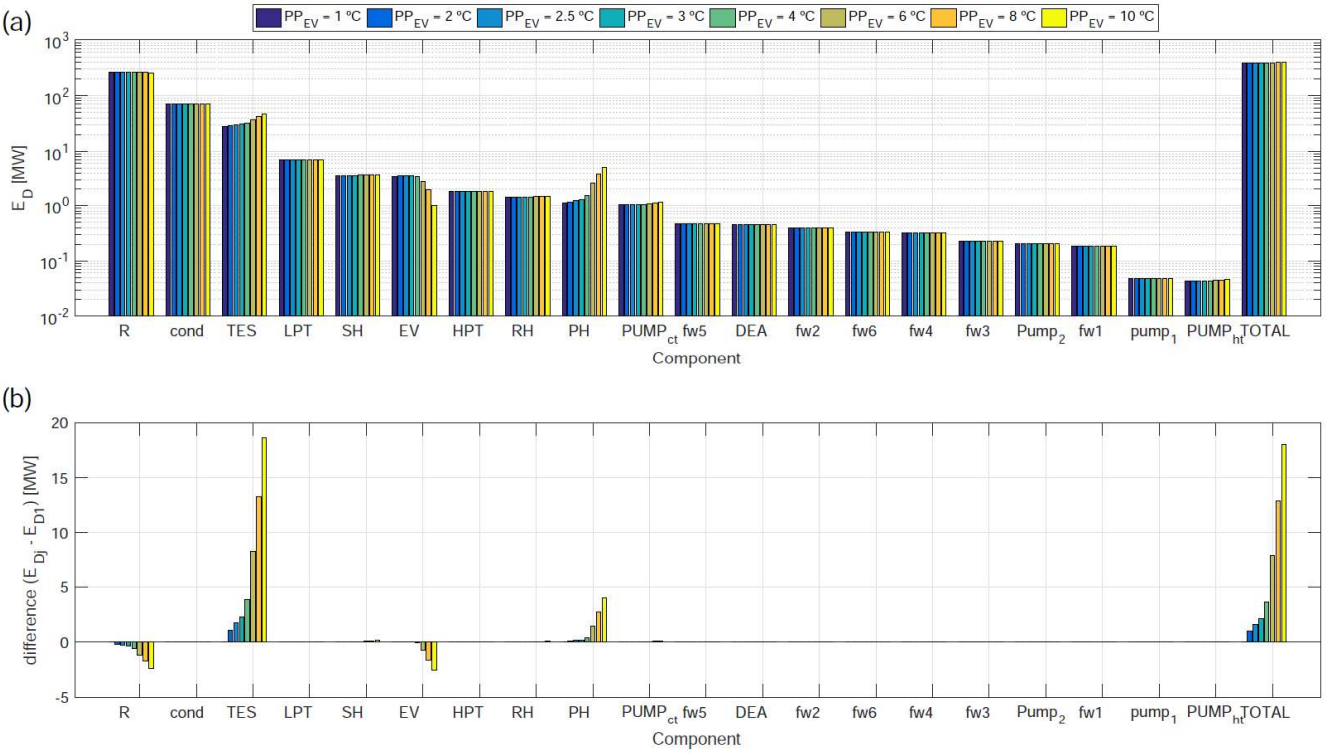

Figure 8. Exergy results: (a) Exergy destruction rate for each component and (b) difference of the exergy destructed between each pinch point and PP_{EV} = 1 ºC.

The difference between each pinch point and PP_{EV} = 1 ºC shows the influence of the pinch point on the rate of exergy destruction, Fig. 8-b. In Fig. 8-b, positive values reflect an increase of the exergy destructed as the pinch point increases while negative values identify a reduction of the exergy destructed as the pinch point increase. The results show that the exergy destructed by the components of the power block is independent of the pinch point. This result is clear and expected as the inlet temperatures of the HPT and LPT (T_{SG4} and T_{SG6}) and the inlet salt temperature (T_{S1}) are fixed in this work. Thus, the heat flux from the molten salt is constant, involving the increase of the salt mass-flow rate as the pinch point increases.

However, the pinch point affects the exergy destructed by the components of the solar system. In this sense, the receptor destroys less exergy as the pinch point increases. This can be explained by the increase of the salt mass-flow and the cold storage temperature (T_{S8}), which raises the exergy of the products in the receptor. A different

behavior is shown for the TES system, which destroys more exergy as the pinch point increases. In summary, the result of the overall plant shows that the rate of exergy destruction increases with the pinch point, promoting the plant operation at low pinch point temperatures.

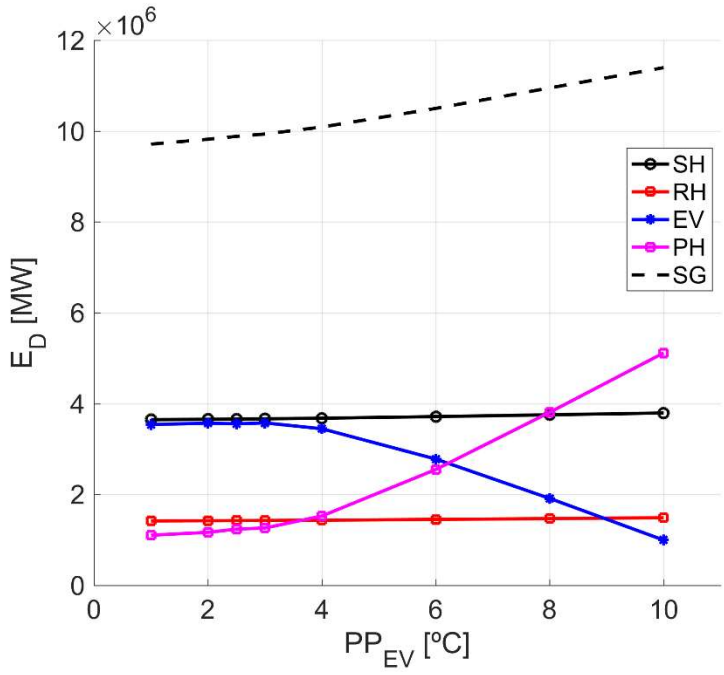

Figure 9. Exergy destruction in the SG heat exchangers versus the pinch point.

Figure 9 further explores the results shown in Fig.8 of the exergy destruction in the SG. The SG heat exchangers show low exergy destruction rate at low pinch point values. This result is produced by the high exergy destructed in the PH and the slight increase in the SH and RH at high pinch point. Only the EV reduces the exergy destruction rate as the pinch point increases. The non-steaming condition imposed in the outlet of the PH produces this result. As the pinch point increases, the approach point increases too [26], reducing the temperature at the outlet of the PH. In this way, the heat flux to the PH is reduced while the heat duty of the EV increases.

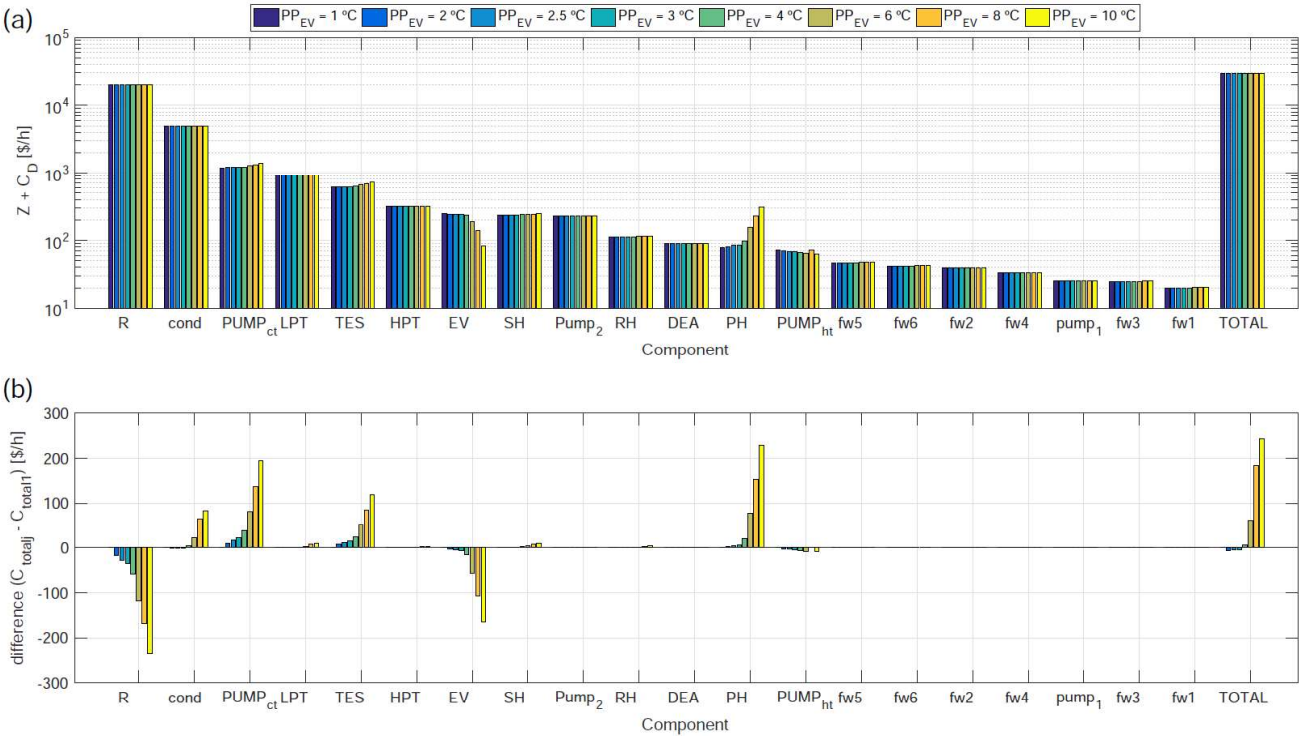

572

573 **Figure 10.** Exergoeconomic results: (a) Total cost rate for each component and (b)
574 difference of the total cost rate between each pinch point and PP_{EV} = 1 ºC.

575 The way that economics are related to thermodynamics is the total cost flow ($\dot{Z} + \dot{C}_D$).
576 This variable is presented in Fig. 10-a for each component. This parameter reflects the
577 cost rate associated to the capital investment and the operating and maintenance costs
578 ($\dot{Z}$), and the cost rate associate to the exergy destruction ($\dot{C}_D$). Similarly to Fig. 8-a, the
579 results are sorted in descending order. In Fig. 10-a, the receiver and the condenser
580 show the highest values of the total cost rate, in a similar way to the exergy destruction
581 results of Fig. 8-a. However, the next component in the cost rate is the cold salt pump,
582 which is caused due to the high operating costs generated by the high salt mass-flow
583 rates that appear when increasing the pinch point. Similar $\dot{Z} + \dot{C}_D$ values are obtained
584 for LPT and TES, while the pinch point markedly influences PH and EV. Lastly, DEA
585 and feedwater heaters show the lowest cost rates together with pump 1.

586 Fig. 10-b shows the cost rate difference between each pinch point and PP_{EV} = 1 ºC.
587 Negative cost rates point to a reduction of the cost flow while positive values mean an

588 increase of the cost rate with the pinch point. Fig. 10-b shows that almost all power
589 block components present negligible changes of the cost rate. Only the condenser cost
590 rate increases with the pinch point temperature. In the solar part, the cost rate of the
591 receiver and EV decreases as the pinch point increases. This result suggests that a
592 higher pinch point would be beneficial for the operation of these devices. However, an
593 opposite effect is shown in the cold pump, TES and PH, in which an increase of the
594 pinch point raises the cost rates associated to these devices. Note that the variation in
595 the PH and EV is explained by the exergy destructed (Fig. 9). Thus, the selection of an
596 optimum pinch point for the plant is a balance of both effects: i) the receiver tendency
597 of operating at high pinch points due to the lower exergy destruction and low cost rate,
598 and ii) the tendency of the cold pump and the rest of components for working at low
599 pinch points.

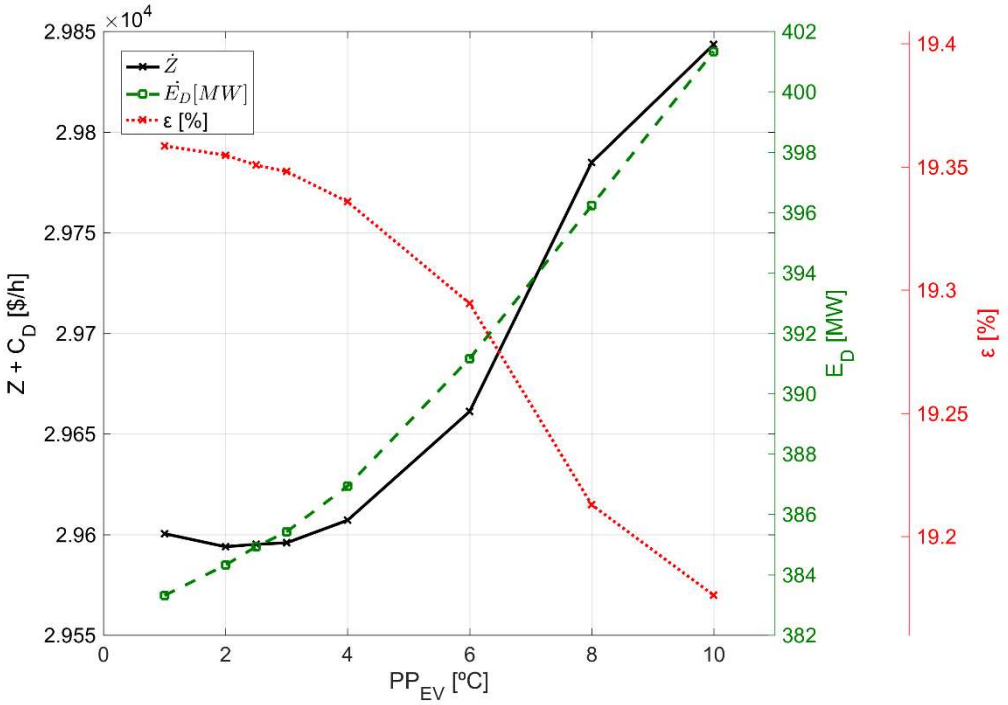

600

601 **Figure 11.** Effect of the pinch point on total cost rate, exergy destruction rate and
602 exergetic efficiency of the plant.

603 The influence of the pinch point on the system performance is studied in Fig. 11. This
604 figure shows a summary of the properties studied, which are the total cost rate, the
605 exergy destruction rate and the exergetic efficiency. Focusing on the exergy results, it
606 is clear that an increase of the pinch point is penalized by an increment of the exergy
607 destructed and by the reduction of the exergetic efficiency, which values are similar to
608 [19, 45]. As was shown in Fig. 8, this is a consequence of the high exergy destructed in
609 the TES. A similar result is obtained from the exergoeconomic analysis, in which the
610 system cost rate shows an optimum value between PP_{EV} = 2 ºC and 3 ºC. In this case,
611 the tendency of working at high pinch point values to minimize $\dot{Z} + \dot{C}_D$ in the receiver is
612 opposed by the effect of the cold pump and the rest of components.

613 Furthermore, it is worth to mention that the optimum pinch point value (PP_{EV} = 2 – 3 ºC)
614 obtained by the exergoeconomic analysis, considering the SPTP, is very close to the
615 optimum pinch point temperature (PP_{EV} = 2.6 ºC) obtained in [26] considering only the
616 SG. The similar result of both methods points out to the meaningful relevance of the
617 pinch point temperature on the overall plant performance, and also, highlights the
618 importance of a proper SG design for the optimum plant operation, as it is seen in
619 Table 6 using the exergoeconomic factor (f).

620 A further analysis of PP_{EV} = 2 ºC is presented in Tables 5 and 6. The state properties,
621 exergies and cost rates are given in Table 5. Table 6 summarizes the exergoeconomic
622 analysis.

623 **Table 5**. Thermodynamic properties, exergy and exergy costs for PP_{EV} = 2 ºC.

State	**PP_{EV} = 2 ºC**						
point	**T [ºC]**	**P [bar]**	**$\dot{m}$ [kg/s]**	**h [kJ/kg]**	**$\dot{E}$ [MW]**	**$\dot{C}$ [$/h]**	**c [$/GJ]**
S1	565.00	10.00	572.05	843.23	204.19	11946.00	16.25
S2	565.00	10.00	389.29	843.23	138.95	8129.10	16.25
S3	447.09	8.52	389.29	662.36	95.05	5560.30	16.25

S4	565.00	10.00	182.77	843.23	65.24	3816.50	16.25
S5	447.09	8.52	182.77	662.52	44.65	2612.30	16.25
S6	447.09	8.52	572.05	662.41	139.70	8172.60	16.25
S7	331.64	7.02	572.05	490.26	85.46	4999.40	16.25
S8	285.10	5.07	572.05	419.01	64.79	3790.60	16.25
S9	285.10	5.07	1304.30	419.01	147.73	3078.30	5.79
S10	286.11	71.48	1304.30	424.05	153.27	4718.10	8.55
S11	565.00	1.50	1304.30	842.52	464.73	12324.00	7.37
S12	565.00	1.50	572.05	842.52	203.83	11847.00	16.15
SG1	244.99	132.00	86.93	1061.60	23.11	2156.90	25.93
SG2	329.23	128.00	86.93	1530.40	42.60	3378.00	22.03
SG3	329.65	128.00	86.93	2663.30	93.27	6586.60	19.62
SG4	550.00	126.00	86.93	3473.30	133.52	9178.60	19.09
SG5	369.00	37.27	78.71	3144.40	93.37	6418.60	19.09
SG6	550.00	35.27	78.71	3564.00	112.53	7651.70	18.89
R1	41.50	0.08	60.12	2383.00	9.21	625.94	18.89
R2	39.48	0.07	72.44	165.01	0.21	13.99	18.89
R3	39.70	17.00	72.44	167.17	0.31	48.04	42.55
R4	59.00	15.00	72.44	247.63	0.83	102.91	34.58
R5	91.80	13.00	72.44	384.94	2.39	248.22	28.90
R6	116.00	11.00	72.44	486.87	4.01	383.71	26.56
R7	144.40	9.00	72.44	607.73	6.39	578.23	25.14
R8	177.47	9.30	86.93	757.51	11.90	1059.70	24.73
R9	181.50	136.00	86.93	775.55	13.27	1393.80	29.18
R10	210.40	134.00	86.93	903.02	17.41	1723.20	27.50
A1	61.14	0.21	2.17	2492.80	0.62	42.20	18.89
A2	108.00	0.79	3.74	2694.40	1.85	125.71	18.89

A3	183.60	1.81	2.89	2838.20	1.88	127.59	18.89
A4	266.20	4.21	3.52	2996.60	2.91	198.00	18.89
A5	367.10	9.30	4.30	3195.30	4.44	301.68	18.89
A6	457.10	18.54	3.97	3375.00	4.87	331.28	18.89
A7	368.00	35.61	6.21	3145.40	7.34	504.59	19.09
V1	216.00	132.00	6.21	928.12	1.31	89.75	19.09
V2	187.10	18.54	10.19	794.18	1.54	104.38	18.89
V3	121.60	4.21	3.52	510.13	0.21	14.53	18.89
V4	97.40	1.81	6.41	407.64	0.23	15.95	18.89
V5	64.60	0.79	10.15	269.86	0.13	8.90	18.89
V6	45.30	0.21	12.32	189.07	0.05	3.59	18.89

Focusing on the exergoeconomic factor (Table 6), salt and water pumps show the highest values due to the low costs of exergy destruction. Similar values are obtained in the literature [1]. Following with the solar field and the receiver, a value of $f = 54.43\%$ is obtained. This means that, in spite of the high exergy destruction, the capital investment and maintenance costs have a similar value to the costs of exergy destruction. A high value of $f = 87.46\%$ points that the cost rate of exergy destruction in the TES system is low. Lower exergoeconomic factors are obtained for both turbines, especially in LPT due to the high number of vapor extractions that increase the exergy destructed up to $\dot{E}_D = 7.01\ MW$ while HPT shows lower values of $\dot{E}_D = 1.80\ MW$.

The heat exchangers show the lowest f values. Low pressure feedwater heaters present f values around 30%, while high pressure feedwater heaters show higher values. These heat exchangers are limited to a gradual increase of the water temperature that ensures a low entropy generation, and thus, low rate of exergy destruction ($\dot{E}_D$) with the inconvenience of a relatively high exergy destruction cost ($\dot{C}_D$)

compared to $\dot{Z}$. This gradual increase of the temperature depends on the number of extractions of the LPT and HPT. For the plant layout analyzed, f values are around the expected results [1].

From the cost rate of exergy destruction, the critical heat exchangers of the plant are placed in the steam generator. SH, EV, PH and RH show low f values, especially for the SH and the EV. The low f values indicate a high cost of the exergy destruction, which could be improved changing the operating conditions of the plant to reduce $\dot{C}_D$ of the SG or improving the SG design. A possible option could be the change of the power block working conditions by increasing the pressure of the EV and SH, and thus, changing the inlet pressure to the HPT. This modification would imply a re-design of the HPT. The exergoeconomic analysis reveals that special efforts should be made in the SH and the EV. PH should be also considered in the SG improvement due to the low f value and the high influence of the pinch point temperature on $\dot{Z} + \dot{C}_D$ results (Fig. 11).

Finally, the condenser shows a very low f value due to its high costs of the exergy destruction and the very low capital investment and maintenance costs. Hence, this component could be improved by increasing its exergetic efficiency changing the operating conditions of the cooling fluid.

Table 6. Exergoeconomic results for PP_{EV} = 2 ºC.

Component	ε **[%]**	$\dot{E}_D$ **[MW]**	c_F **[€/GJ]**	c_P **[€/GJ]**	$\dot{Z}$ **[$/h]**	$\dot{C}_D$ **[$/h]**	$\dot{Z} + \dot{C}_D$ **[$/h]**	f **[%]**
SF + R	56.61	260.73	0.00	6.78	7606.00	6367.00	13973.00	54.43
TES	65.74	29.23	7.37	0.65	477.01	68.42	545.42	87.46
$PUMP_{HT}$	89.51	0.04	21.84	75.10	66.46	3.36	69.81	95.19
SH	91.67	3.66	16.25	17.89	23.30	213.93	237.24	9.82
EV	93.41	3.57	16.25	17.59	35.33	208.96	244.29	14.46

PH	94.35	1.17	16.25	17.40	12.29	68.32	80.61	15.24
RH	93.08	1.42	16.25	17.88	28.98	83.31	112.29	25.81
$PUMP_{CT}$	84.26	1.03	21.84	82.27	1123.10	81.33	1204.40	93.25
$PUMP_1$	68.90	0.05	21.84	42.54	21.74	3.83	25.57	85.03
FW1	73.42	0.19	18.88	29.70	7.36	12.62	19.98	36.84
FW2	79.85	0.39	18.88	25.89	12.56	26.75	39.31	31.96
FW3	87.70	0.23	18.88	23.12	9.33	15.52	24.84	37.54
FW4	88.07	0.32	18.88	22.73	11.06	21.88	32.94	33.57
DEA	96.30	0.46	9.12	11.23	75.36	15.03	90.40	83.37
$PUMP_2$	87.02	0.20	21.84	29.17	210.81	16.00	226.80	92.95
FW5	89.87	0.47	18.88	22.02	14.05	31.73	45.77	30.69
FW6	94.43	0.34	19.09	21.06	17.47	23.08	40.55	43.07
HPT	93.93	1.80	21.84	21.84	176.94	141.83	318.77	55.51
LPT	92.20	7.01	21.84	21.84	378.73	551.00	929.72	40.74
COND	11.17	72.01	0.00	18.77	2.93	4866.20	4869.10	0.06
Overall system	19.35	384.32	-	-	10310.79	12820.1	23130.82	44.58

6. Conclusions

In this work, the influence of the SG on a solar power tower plant is presented. It has been observed that the pinch point modifies the operating conditions (salt mass flow, cold storage temperature and pressure drops) of the power plant, the SG design and the capital investment costs of the SG. Such changes in the steam generator design have been used as input data of the thermodynamic and exergoeconomic analyses.

Counter-current U-shell/U-tube heat exchangers design is used for RH and SH, while a straight shell U-tube is proposed for PH and EV. The optimization algorithm used to design the SG shows a significant difference between the costs of PH and the rest of heat exchangers. High pinch point values reduce significantly PH costs, although this

reduction in area increases the salt mass flow and the operating costs of the salt pumps.

A great proportion of the exergy destructed occurs in the solar receptor, the condenser and the thermal storage system due to the high heat fluxes in these components. The increase of the mass flow rate of molten salt in the solar receiver together with the increase of the temperature of the cold tank, which is the inlet temperature of the receiver, increases the exergy destructed in the plant. Thus, low pinch point values present the lowest rate exergy destruction for the plant. Due to that, the maximum exergetic efficiency of the plant is obtained for a pinch point of 1ºC.

The exergoeconomic approach provides a different view of the system behavior. Focusing on the pinch point influence on the system components, the steam generator, which design depends on the pinch point, has confirmed as the critical part of the solar power tower plant. The change of the plant operating conditions, such as the inlet temperature of the receiver or the salt mass flow, mainly affects to the superheater, evaporator and preheater. The low exergoeconomic factors (f) shown for these heat exchangers encourage the change of the plant operating conditions to reduce the cost rate of exergy destruction. This could be achieved by the increase of the inlet pressure in the evaporator and superheater, modifying the working conditions of the high pressure turbine, and further optimizing the plant operation. For the conditions considered in this study, with a constant operation of the power block at 110 MWe, a pinch point of 2 - 3 ºC would be the optimum to design the solar tower plant.

Acknowledgments

This work has been supported by the Spanish Government under the project ENE2015-69486-R (MINECO/FEDER, UE).

7. References

[1] A. Bejan, G. Tsatsaronis, M. J. Moran, Thermal Design and Optimization, John Wiley &

696 Sons Inc. (1996).

697 [2] G. Tsatsaronis, M. J. Moran, Exergy-aided cost optimization, Energy Convers. Manag. 38
698 (1997) 1535-1542.

699 [3] M. J. Moran, H. N. Shapiro, H. N. Fundamentals of engineering thermodynamics. John
700 Wiley & Sons Inc. (2010).

701 [4] A. Valero, M. A. Lozano, M. Muñoz, A general theory of exergy saving. I. On the
702 exergetic cost. Compu. Aided Eng. 3 (1986) 1-8.

703 [5] A. Valero, M. A. Lozano, M. Muñoz, A general theory of exergy saving. II. On the
704 thermoeconomic cost. Compu. Aided Eng. 3 (1986) 9-115.

705 [6] R. Kumar, A critical review on energy, exergy, exergoeconomic and economic (4-E)
706 analysis of thermal power plants, Eng. Sci. Technol. 20 (2017) 283-292.

707 [7] M. A. Rosen, I. Dincer, Exergoeconomic analysis of power plants operating on various
708 fuels, Appl. Therm. Eng. 23 (2003) 643–658.

709 [8] J.L. Silveira, C.E. Tuna, Thermoeconomic analysis method for optimization of combined
710 heat and power systems. Part I, Prog. Energy Combust. Sci. 29 (2003) 479-485.

711 [9] M. Ameri, P. Ahmadi, A. Hamidi, Energy, exergy and exergoeconomic analysis of a
712 steam power plant: A case study. Int. J. Energy Res., 33 (2009) 499–512.

713 [10] R. Carapellucci, L. Giordano, A comparison between exergetic and economic criteria for
714 optimizing the heat recovery steam generators of gas-steam power plants, Energy. 58
715 (2013) 458-472.

716 [11] S. Khanmohammadi, A. R. Azimian, Exergoeconomic Evaluation of a Two-Pressure Level
717 Fired Combined-Cycle Power Plant, J. Energy Eng. 141 (2015) (3): 04014014.

718 [12] A. Ganjehkaviri, M. N. M. Jaafar, S. E. Hosseini, Optimization and the effect of steam
719 turbine outlet quality on the output power of a combined cycle power plant, Energy
720 Conv. Manag. 89 (2015) 231–243.

721 [13] P. Ifaei, A. Ataei, C. Yoo, Thermoeconomic and environmental analyses of a low water
722 consumption combined steam power plant and refrigeration chillers-Part 2 :
723 Thermoeconomic and environmental analysis, Energy Conv. Manag. 123 (2016) 625–
724 642.

725 [14] H. Nami, S.M.S. Mahmoudi, A. Nemati, Exergy, economic and environmental impact
726 assessment and optimization of a novel cogeneration system including a gas turbine, a
727 supercritical CO_2 and an organic Rankine cycle (GT-HRSG/SCO_2), Appl. Therm. Eng. 110
728 (2017) 1315-1330.

729 [15] A. Baghernejad, M. Yaghoubi, Exergoeconomic analysis and optimization of an
730 Integrated Solar Combined Cycle System (ISCCS) using genetic algorithm. Energy Conv.
731 Manag. 52 (2011) 2193–2203.

732 [16] A. Baghernejad, M. Yaghoubi, Multi-objective exergoeconomic optimization of an
733 Integrated Solar Combined Cycle System using evolutionary algorithms, Int. J. Energy
734 Res. 35 (2011) 601–615.

735 [17] P. Habl, A. M. Blanco-Marigorta, B. Erlach, Exergoeconomic comparison of wet and dry
736 cooling technologies for the Rankine cycle of a solar thermal power plant, Proceedings
737 of the 25th International Conference on Efficiency, Cost, Optimization and Simulation of
738 Energy Conversion Systems and Processes, 3 (2012) 109-122.

739 [18] A. M. Elsafi, Exergy and exergoeconomic analysis of sustainable direct steam generation
740 solar power plants, Energy Conv. Manag. 103 (2015) 338–347.

741 [19] C. Xu, Z. Wang, X. Li, F. Sun, Energy and exergy analysis of solar power tower plants,
742 Appl. Therm. Eng. 31 (2011) 3904–3913.

743 [20] Modi, A., & Haglind, F.. Performance analysis of a Kalina cycle for a central receiver
744 solar thermal power plant with direct steam generation, Appl. Therm. Eng. 65(1–2),
745 201–208.

746 [21] R. Soltani, P. M. Keleshtery, M. Vahdati, M. H. Khoshgoftarmanesh, M. A. Rosen, M.
747 Amidpour, Multi-objective optimization of a solar-hybrid cogeneration cycle:
748 Application to CGAM problem, Energy Conv. Manag. 81 (2014) 60–71.

749 [22] K. Wang, Y. He, Thermodynamic analysis and optimization of a molten salt solar power
750 tower integrated with a recompression supercritical CO_2 Brayton cycle based on
751 integrated modeling, Energy Conv. Manag. 135 (2017) 336–350.

752 [23] A. Kouta, F. Al-sulaiman, M. Atif, S. Bin, Entropy, exergy, and cost analyses of solar
753 driven cogeneration systems using supercritical CO_2 Brayton cycles and MEE-TVC
754 desalination system. Energy Conv. Manag. 115 (2016) 253–264.

755 [24] M.H. Khoshgoftar Manesh, M. Ameryan, Optimal design of a solar-hybrid cogeneration
756 cycle using Cuckoo Search algorithm, Appl. Therm. Eng. 102 (2016) 1300-1313.

757 [25] C. Toro, M. V. Rocco, E. Colombo, Exergy and thermoeconomic analyses of central
758 receiver concentrated solar plants using air as heat transfer fluid, Energies. 9 (2016)
759 885.

760 [26] P. A. Gónzalez-Gómez, J. Gómez-Hernández, J. Villa Briongos, D. Santana, Thermo-
761 economic optimization of molten salt steam generators, Energy Conv. Manag. 146
762 (2017) 228-243.

763 [27] TEMA Report, Standards of the Tubular Exchangers Manufacturers Association, (2007).

764 [28] American Society of Mechanical Engineers. ASME boiler and pressure vessel code,
765 Section VIII, (2010).

766 [29] National Renewable Energy Laboratory (NREL), (2016).
767 http://www.nrel.gov/csp/solarpaces/by_project.cfm.

768 [30] I. H. Bell, J. Wronski, S. Quoilin, V. Lemort, Pure and Pseudo-pure Fluid Thermophysical
769 Property Evaluation and the Open-Source Thermophysical Property Library CoolProp,
770 Ind. Eng. Chem. Res. 53 (2014) 2498-2508. www.coolprop.org.

771 [31] R. Ferri, A. Cammi, D. Mazzei, Molten salt mixture properties in RELAP5 code for
772 thermodynamic solar applications, Int. J. Therm. Sci. 47 (2008) 1676–1687.

773 [32] B. D. Iverson, S. T. Broome, A. M. Kruizenga, J. G. Cordaro, Thermal and mechanical
774 properties of nitrate thermal storage salts in the solid-phase, Solar Energy. 86 (2012)
775 2897–2911.

776 [33] C. K. Ho, B. D. Iverson, Review of high-temperature central receiver designs for
777 concentrating solar power. Renewable Sustainable Energy Rev. 29 (2014) 835-846.

778 [34] Natl. Renewable Energy Lab., Thermal Storage Commercial Plant Design Study for a 2-
779 Tank Indirect Molten Salt System, Natl. Renewable Energy Lab. Report NREL/SR-550-
780 40166, (2006).

781 [35] M. R. Rodriguez-Sanchez, A. Sanchez-Gonzalez, D.Santana, Revised receiver efficiency
782 of molten-salt power towers, Renewable Sustainable Energy Rev. 52 (2015) 1331-1339.

783 [36] P.A. González-Gómez, F. Petrakopoulou, J.V. Briongos, D. Santana, Cost-based design
784 optimization of the heat exchangers in a parabolic trough power plant, Energy. 123

785 (2017) 314–325.

786 [37] W. J. O'Donnell, B. F. Langer. Design of perforated plates, J. Eng. Ind. 84 (1982) 307-19.

787 [38] J. Busuttil, Detailed stress analysis of SM-1 steam generator tube sheet. ALCO Products
788 Inc (1962).

789 [39] M. A. Rosen, I. Dincer, Effect of varying dead-state properties on energy and exergy
790 analyses of thermal systems, Int. J. Therm. Sci. 43 (2004) 121–133.

791 [40] A. Acir, A. K. Bilginsoy, H. Coşkun, Investigation of varying dead state temperatures on
792 energy and exergy efficiencies in thermal power plant, J. Energy Inst. 85 (2012) 14-21.

793 [41] M. Sharma, O. Singh, Exergy analysis of dual pressure HRSG for different dead states
794 and varying steam generation states in gas/steam combined cycle power plant, Appl.
795 Therm. Eng. 93 (2016) 614-622.

796 [42] M. A. Lozano, A. Valero, Theory of the exergetic cost, Energy, 18 (1993) 939-960.

797 [43] R. Petela, Exergy of heat radiation. ASME J Heat Transf. 68 (1964) 187–92.

798 [44] S. A. Kalogirou, S. Karellas, K. Braimakis, C. Stanciu, Exergy analysis of solar thermal
799 collectors and processes. Prog. Energy Combust. Sci. 56 (2016) 106-137.

800 [45] S. Giuliano, R. Buck, S. Eguiguren, Analysis of Solar-Thermal Power Plants With Thermal
801 Energy Storage and Solar-Hybrid Operation Strategy, J. Sol. Energy Eng. 133 (2011)
802 031007-031007-7.

803 [46] A. Rovira, M. J. Montes, M. Valdes, J. M. Martínez-Val, F. Varela, On the improvement
804 of annual performance of solar thermal power plants through exergy management, Int.
805 J. Energy Res. 38 (2014) 658 – 673.

[47] D. Cocco, M. Petrollese, V. Tola, Exergy analysis of concentrating solar systems for heat and power production, Energy, 130 (2017) 192-203.

[48] A. Lazzaretto, G. Tsatsaronis, SPECO: a systematic and general methodology for calculating efficiencies and costs in thermal systems, Energy, 31 (2006) 1257-1289.

[49] A. L. Avila-Marin, J. Fernandez-Reche, F. M. Tellez, Evaluation of the potential of central receiver solar power plants: Configuration, optimization and trends, Applied Energy, 112 (2013) 274–288.

[50] G.P. Purohit, Estimating costs of shell-and-tube heat exchangers, Chem. Eng. (1983) 56–67.

[51] Natl. Renewable Energy Lab., Molten salt power tower cost model for the System Advisor Model, Natl. Renewable Energy Lab. Report, NREL/SR-5500-57625, (2013).